Published in final edited form as:
Biochem J. 2008 May 1; 411(3): 485–493. doi:10.1042/BJ20071546.

The guanine-nucleotide-exchange factor BopE from *Burkholderia pseudomallei* adopts a compact version of the *Salmonella* SopE/SopE2 fold and undergoes a closed-to-open conformational change upon interaction with Cdc42

Abhishek Upadhyay[*,1], **Huan-Lin Wu**[*,1], **Christopher Williams**[*,2], **Terry Field**[†], **Edouard E. Galyov**[†,3], **Jean M. H. Van Den ELSEN**[*], and **Stefan Bagby**[*,4]

[*]Department of Biology and Biochemistry, University of Bath, Bath BA2 7AY, U.K.

[†]Division of Environmental Microbiology, IAH (Institute for Animal Health), Compton Laboratory, Berkshire RG20 7NN, U.K.

Abstract

BopE is a type III secreted protein from *Burkholderia pseudomallei*, the aetiological agent of melioidosis, a severe emerging infection. BopE is a GEF (guanine-nucleotide-exchange factor) for the Rho GTPases Cdc42 (cell division cycle 42) and Rac1. We have determined the structure of BopE catalytic domain (amino acids 78–261) by NMR spectroscopy and it shows that $BopE_{78-261}$ comprises two three-helix bundles ($\alpha1\alpha4\alpha5$ and $\alpha2\alpha3\alpha6$). This fold is similar to that adopted by the BopE homologues SopE and SopE2, which are GEFs from *Salmonella*. Whereas the two three-helix bundles of $SopE_{78-240}$ and $SopE_{269-240}$ form the arms of a 'Λ' shape, $BopE_{78-261}$ adopts a more closed conformation with substantial interactions between the two three-helix bundles. We propose that arginine and proline residues are important in the conformational differences between BopE and SopE/E2. Analysis of the molecular interface in the $SopE_{78-240}$–Cdc42 complex crystal structure indicates that, in a BopE–Cdc42 interaction, the closed conformation of $BopE_{78-261}$ would engender steric clashes with the Cdc42 switch regions. This implies that $BopE_{78-261}$ must undergo a closed-to-open conformational change in order to catalyse guanine nucleotide exchange. In an NMR titration to investigate the $BopE_{78-261}$–Cdc42 interaction, the appearance of additional peaks per NH for residues in hinge regions of $BopE_{78-261}$ indicates that $BopE_{78-261}$ does undergo a closed-to-open conformational change in the presence of Cdc42. The conformational change hypothesis is further supported by substantial improvement of $BopE_{78-261}$ catalytic efficiency through mutations that favour an open conformation. Requirement for closed-to-open conformational change explains the 10–40-fold lower k_{cat} of BopE compared with SopE and SopE2.

[4]To whom correspondence should be addressed (email bsssb@bath.ac.uk)..
[1]These authors contributed equally to this work.
[2]Present address: School of Chemistry, University of Bristol, Cantock's Close, Bristol BS8 1TS, U.K.
[3]Present address: Department of Infection, Immunity and Inflammation, Medical Sciences Building, University of Leicester, PO Box 138, Leicester LE1 9HN, U.K.

BopE atomic co-ordinates and NMR restraints have been deposited in the PDB (http://www.rcsb.org) under the codes 2JOK and 2JOL. BopE chemical shifts have been deposited in Biological Magnetic Resonance Bank (http://www.bmrb.wisc.edu) under the code BMRB-5974.

Keywords

bacterial pathogen; guanine-nucleotide-exchange factor; protein–protein interaction; protein structure; Rho GTPase; type III secretion

INTRODUCTION

Burkholderia pseudomallei is a Gram-negative bacterium that is the aetiological agent of melioidosis, a severe emerging infection of humans and animals that is endemic in South-East Asia and tropical Australia and that has the potential to spread worldwide [1-3]. Melioidosis has a range of clinical manifestations, including rapidly fatal septicaemia, pneumonia, skin and soft tissue abscesses, and osteomyelitis or septic arthritis. Infection is usually via contaminated soil, dust or water [4-6]. Asymptomatic infection is common in areas where the infection is endemic and progression to disease depends on the condition of the host [5]. Between the fatal and asymptomatic extremes, the infection may be chronic or may run a relapsing course. Latency and relapse are common even in patients treated with appropriate antibiotics [7]. *B. pseudomallei* is closely related to *Burkholderia mallei*, the pathogen that causes glanders, a disease of horses and other solipeds. *B. mallei* can also affect humans and is often fatal if left untreated [8]. Due to the severity of the infection, aerosol infectivity and worldwide availability, both *B. pseudomallei* and *B. mallei* are considered to be potential bio-weapons [9]. There is currently no vaccine against *B. pseudomallei* [10].

The molecular mechanisms of *B. pseudomallei* pathogenesis are not completely understood [11]. *B. pseudomallei* has a 7.3 Mb genome, unusually large for a prokaryote, comprising two chromosomes with 16 genomic islands possibly acquired through very recent lateral transfer [12]. The *B. pseudomallei* genome contains at least three loci encoding putative TTS systems (type III secretion systems) [13]. One of these, Bsa, is homologous with the inv/spa/prg TTS system of *Salmonella* serotype Typhimurium [13-15]. TTS systems resemble molecular syringes for the injection of multiple bacterial effector proteins into the host cell cytoplasm that modify host cell physiology to the benefit of the pathogen [16,17]. TTS systems are central to the virulence of many Gram-negative pathogens, including *Salmonella*, *Shigella*, *Yersinia,* enteropathogenic *Escherichia coli* and the four major genera of plant pathogenic bacteria [18,19].

BopE, encoded within the Bsa locus, is secreted via the Bsa TTS system and influences invasion of HeLa cells probably via its function as a GEF (guanine-nucleotide-exchange factor) for Rho GTPases that regulate the actin network [20]. BopE shares sequence homology with the *Salmonella* translocated effector proteins SopE [21,22] and SopE2 [23,24] (Supplementary Figure S1 at http://www.BiochemJ.org/bj/411/bj4110485add.htm), which play an important role in *Salmonella* invasion of non-phagocytic intestinal epithelial cells. SopE is a potent GEF for the mammalian Rho GTPases Cdc42 (cell division cycle 42) and Rac1 *in vitro* and *in vivo*, whereas SopE2 efficiently activates Cdc42 but not Rac1 [25]. The structures of SopE [26] and SopE2 [27] are entirely different from those of the best characterized eukaryotic GEFs, which comprise a catalytic DH (Dbl homology) domain and an adjacent PH (pleckstrin homology) domain [28-30], although there are similarities in the catalytic mechanisms [31].

We have previously shown that BopE is monomeric in aqueous solution, adopts a single conformation that is predominantly α-helical, is stable over a wide range of pH values and is able to refold independently [32]. Now, as part of our examination of the structural and mechanistic relationships between BopE and its counterparts SopE and SopE2 from

Europe PMC Funders Author Manuscripts

Salmonella, we report here the three-dimensional structure in solution of the catalytic domain of BopE (BopE residues 78–261, where 261 is the C-terminal residue of the full-length protein) and NMR and kinetic analyses of the interaction of $BopE_{78-261}$ with the Rho GTPase Cdc42.

EXPERIMENTAL

Biophysical and biological characterization, NMR sample generation and NMR spectroscopy of recombinant $BopE_{78-261}$

The methods used to obtain $BopE_{78-261}$ NMR samples and to derive backbone and side-chain resonance assignment, plus biophysical characteristics of $BopE_{78-261}$, have been described previously [32,33]. The ^{1}H, ^{13}C and ^{15}N chemical shifts of $BopE_{78-261}$ are in the BioMagResBank database (http://www.bmrb.wisc.edu) under accession number BMRB-5974. The biological activity of exactly the same $BopE_{78-261}$ construct as used here has been demonstrated previously: $BopE_{78-261}$ was shown to have guanine nucleotide-exchange activity towards Cdc42 and Rac1 *in vitro*[20].

All NMR data were acquired at 25°C on a Varian Unity INOVA spectrometer operating at a nominal proton frequency of 600 MHz, using a triple resonance 5 mm probe equipped with *z*-axis pulsed field gradients. NMR data were processed using the NMRPipe/NMRDraw software suite [34] and analysed using the SPARKY assignment program (http://www.cgl.ucsf.edu/home/sparky/). NOE (nuclear Overhauser effect) distance restraints were obtained by analysis of ^{1}H-^{1}H two-dimensional NOESY [36] (100 and 175 ms mixing times), ^{15}N-NOESY HSQC (heteronuclear single-quantum coherence) [37] (50, 100 and 150 ms mixing times) and simultaneous three-dimensional $^{15}N/^{13}C$-edited NOESY [38] (100 ms mixing time) spectra. Backbone $^{1}D_{NH}$ RDC (residual dipolar coupling) restraints were measured for $BopE_{78-261}$ aligned with respect to the magnetic field by using a stretched polyacrylamide gel; gels were made using an apparatus based on that described previously [39]. RDCs were measured using IPAP (in-phase anti-phase)–HSQC [40].

Structure calculation

Each NOE was assigned to one of four restraint distances based on the peak intensity: 1.8–2.8, 1.8–3.3, 1.8–5.0 and 1.8–6.0 Å (1 Å = 0.1 nm), corresponding to strong, medium, weak and very weak NOEs. Distances involving methyl groups, aromatic ring protons and non-stereospecifically assigned methylene protons were represented as a $(\Sigma r^{-6})^{-1/6}$ sum [41]. For strong and medium NOE restraints involving amide protons, 0.2 Å was added. Backbone dihedral angles φ and ψ were predicted from $^{13}C_{\alpha}$, $^{13}C_{\beta}$, $^{13}C'$, $^{1}H_{\alpha}$ and backbone ^{15}N chemical shifts using TALOS [42]. The φ dihedral angles were restrained to TALOS-predicted values ±30° for α-helices and ±40° for β-strands and ψ dihedral angles were restrained to TALOS-predicted values ±50°. Hydrogen bond restraints were obtained from hydrogen–deuterium exchange experiments: uniformly ^{15}N-labelled $BopE_{78-261}$ in NMR buffer was freeze-dried and resuspended in 99.96 % $^{2}H_2O$. A series of ^{1}H-^{15}N HSQC spectra was then recorded to determine amide protons protected from exchange with the solvent. For hydrogen bond distance constraints, the NH–O distance was assigned lower and upper distance bounds of 1.5 and 2.5 Å, and the N–O distance was assigned lower and upper distance bounds of 2.5 and 3.5 Å.

Structures were calculated using the Python interface of Xplor-NIH 2.16.0 [43,44], using simulated annealing starting from random extended structures. Default values were used for all force constants and molecular parameters. The ensemble of NMR structures was analysed for violated restraints using the VMD-Xplor visualization package [45]. The structure determination was carried out iteratively whereby consistently violated restraints

were reassigned, wherever possible, using existing structures or removed until a consistent set of constraints was obtained with few violations in the ensemble. The ensemble of structures was further refined with Xplor-NIH standard refinement protocols by using the final set of restraints. The quality of the structures was assessed by using PROCHECK-NMR [46].

NMR titration of Cdc42Δ7 against $BopE_{78-261}$

Binding of unlabelled human Cdc42Δ7to ^{15}N-labelled $BopE_{78-261}$ was monitored by recording ^{1}H-^{15}N HSQC spectra as a function of the $BopE_{78-261}$/Cdc42Δ7 ratio. Cdc42Δ7 is Cdc42 lacking seven C-terminal amino acids; it was shown previously that C-terminal truncation of Cdc42 does not interfere with SopE GEF activity [47]. Cdc42Δ7 was purified from *E. coli* BL21(DE3) as previously described [47]. The NMR titration was performed as previously described [27,48]. Briefly, two initial NMR samples were prepared in 0.5 ml of NMR buffer (20 mM sodium phosphate, pH 5.5, and 50 mM NaCl) with 10 % $^{2}H_2O$. Sample A contained 0.5 mM ^{15}N-labelled $BopE_{78-261}$ (1.0:0.0 molar ratio of $BopE_{78-261}$/ Cdc42Δ7) and sample B contained 0.5 mM ^{15}N-labelled $BopE_{78-261}$ and 1.34 mM Cdc42Δ7 (1.0:2.7 molar ratio of $BopE_{78-261}$/Cdc42Δ7). The buffer composition of both samples was identical as both samples were extensively exchanged into the same batch of sample buffer. Throughout the titration, the concentration of $BopE_{78-261}$ was maintained at a constant concentration of 0.5 mM and the Cdc42Δ7 concentration was varied to give a series of $BopE_{78-261}$/Cdc42Δ7 molar ratios from 1.0:0.0 to 1.0:2.7. A ^{1}H-^{15}N HSQC spectrum was acquired at each titration point with 512 complex ^{1}H points and 192 complex ^{15}N points with 32 scans per increment and spectral widths of 8000 Hz in ^{1}H and 2000 Hz in ^{15}N. The initial NMR samples represented the end points of the titration. Intermediate values of $BopE_{78-261}$/Cdc42Δ7 were obtained by simultaneously taking equal aliquots from both sample A and sample B and then transferring the aliquots to the other NMR tube (i.e. from tube A to tube B and vice versa). This procedure was repeated until a series of 12 ^{1}H-^{15}N HSQC experiments at $BopE_{78-261}$/Cdc42Δ7 molar ratios between 1.0:0.0 and 1.0:2.7 was completed.

Generation and characterization of BopE mutants

$BopE_{78-261}$ double mutants N224P/R230Q (mutant 1), N216P/ L226P (mutant 2) and R207E/N216P (mutant 3) were made using the following pairs of primers (shown as 5′–3′; ‘for’ is forward; ‘rev’ is reverse): TCGCCCACGCTCGTCGAGTTCCAGCAGACGGT (N224PR230Q for) and CTGCTGGAACTCGACGAGCGTGGGCGAACGCTC (N224PR230Q rev); CGCCCGCGTTGCCGGCCGAGCGTTCGAACACGCCCGTCGAGT (N216PL226P for) and ACGGGCGTGTTCGAACGCTCGGCCGGCAACGCGGGCGCGACGA (N216PL226P rev); TGCGGAGCAGCAGGCGATCGATCTCGTCGCGCCCGCGTTGCC (R207EN216P for) and CGCGGGCGCGACGAGATCGATCGCCTGCTGCTCCGCATAC (R207EN216P rev). The mutants were constructed by overlapping PCR. The two overlapping primers (for and rev) were used in PCR with upstream and downstream primers to amplify the two parts of the gene (upstream-rev and for-downstream respectively). The resulting DNA fragments were purified, mixed and used as a template for a third PCR with upstream and downstream primers to amplify the mutated gene. The resulting DNA fragment in each case was digested with EcoRI and BamHI and cloned into pGEX4T1 (GE Healthcare). The cloned DNA was then sequenced. The mutant proteins were expressed and purified in the same way as wild-type $BopE_{78-261}$ [32].

Filter binding assays

Cdc42Δ7 was loaded at 25°C for 10 min with [^{3}H]GDP in a reaction buffer containing 30 mM Hepes, 100 mM KCl, 0.1 mM EDTA (pH 7.5), 1 μg of creatine phosphokinase (Sigma)

and 0.5 mM DTT (dithiothreitol). $MgCl_2$ was added to a final concentration of 2.8 mM and the mixture was incubated for another 2 min. Exchange reactions were started by adding the respective GEF and unlabelled GDP to the reaction mixture containing Cdc42Δ7 and [^{3}H]GDP. BSA (Sigma) was used as a negative control and $SopE2_{69-240}$ was used as a positive control. Aliquots were withdrawn and the reaction was stopped by quenching in ice-cold wash buffer, containing 30 mM Hepes, 100 mM KCl, 0.1 mM EDTA and 5 mM $MgCl_2$ (pH 7.5), followed by analysis with the nitrocellulose filter binding assay [49]. Filters were washed twice with wash buffer, containing 30 mM Hepes, 100 mM KCl, 0.1 mM EDTA and 5 mM $MgCl_2$ (pH 7.5) and dried, and the radioactivity bound to the filters was analysed by scintillation counting in a Tri-Carb liquid-scintillation counter 1600 TR (Packard, Meriden, CT, U.S.A.).

RESULTS AND DISCUSSION

Structure determination of $BopE_{78-261}$

A semi-automated procedure for iterative NOE assignment was used to generate the structure of $BopE_{78-261}$. The final structures were generated using 2452 NOE-derived distance restraints (comprising 784 intraresidue, 1151 sequential and medium-range and 517 long-range NOEs, where 'long range' means they are five or more amino acids apart in the sequence), 192 hydrogen bond restraints, 255 φ and ψ dihedral angle restraints (132 φ and 123 ψ) and 98 backbone $^1D_{NH}$ RDC restraints (Table 1). The ensemble of 20 final simulated annealing structures, selected from 40 calculations on the basis of the lowest energy, and the average structure are shown in Figure 1. Over the regular secondary-structure elements, the ensemble of structures has a backbone RMSD (root mean square deviation) from the mean of 0.65 Å and an RMSD of 1.13 Å for all non-hydrogen atoms. A Ramachandran plot of the structures with PROCHECK-NMR [46] indicates that 96.7 % of the residues (excluding glycine and proline residues) lie in the most favoured or additionally allowed regions. The few non-glycine residues to fall into the generously allowed regions and disallowed regions correspond to residues located at the termini or loop regions where the NMR restraint density is low.

Three-dimensional structure of $BopE_{78-261}$ and comparison with *Salmonella* $SopE_{78-240}$ and $SopE2_{69-240}$

BopE has been identified [15] as a homologue of the *Salmonella* effector proteins SopE and SopE2 (Supplementary Figure S1). Overall, BopE has approx. 16 and 17 % sequence identity with SopE and SopE2. Within the catalytic domain (comparing residues 78–240 of SopE and SopE2 with residues 78–240 of BopE), the sequence identity/similarity with SopE and SopE2 is approx. 25 %/40 % and 24 %/39 % respectively.

$BopE_{78-261}$ consists of six major α-helices termed α1 to α6 arranged in two three-helix bundles, $\alpha1\alpha4\alpha5$ and $\alpha2\alpha3\alpha6$. The three-helix bundles are connected by a loop between α1- and α2-helices, a β-hairpin (residues 162–168), followed by a loop that contains the putative (by comparison with SopE, which has a $G^{166}AGA^{169}$ catalytic motif) $G^{171}AGT^{174}$ catalytic motif between α3- and α4-helices, and a loop between α5- and α6-helices (Figure 1).

The $BopE_{78-261}$ fold is similar to that of its *Salmonella* counterparts $SopE_{78-240}$ and $SopE2_{69-240}$, but is more closed and compact with substantial interaction between the two three-helix bundles (Figures 2 and 3). As an illustration of the more extensive association between the bundles in $BopE_{78-261}$, the buried surface areas between the three-helix bundles are 1693 Å^2 in $SopE_{78-240}$, 1849 Å^2 in $SopE2_{69-240}$ and 2148 Å^2 in $BopE_{78-261}$. Also, we have assigned 56 interbundle NOEs in $BopE_{78-261}$ compared with 20 such NOEs in our

previous structure determination of $SopE2_{69-240}$ [27]. The greater conservation of bundle structure relative to bundle–bundle orientation is quantitatively illustrated by RMSD values for superimposed Cα traces and by comparison of interhelical angles. When the catalytic domains are superimposed, the RMSD values are 2.5 Å (SopE versus SopE2), 3.9 Å (SopE2 versus BopE) and 5.0 Å (SopE versus BopE). [Note that the buried surface area and RMSD values plus visual inspection (Figure 2) show that $SopE2_{69-240}$ is somewhat intermediate as it has a slightly more closed conformation than $SopE_{78-240}$; it must be emphasized, however, that the only available $SopE_{78-240}$ structure is from the complex with Cdc42, so it is possible that unbound $SopE_{78-240}$ also has a more closed $SopE2_{69-240}$-like conformation.] When individual three-helix bundles are superimposed, the corresponding values are 2.3, 2.9 and 2.3 Å for the $\alpha1\alpha4\alpha5$ bundle and 1.6, 2.8 and 2.8 Å for the $\alpha2\alpha3\alpha6$ bundle. Calculation of the interhelical angles shows that the angles between helices in different bundles tend to differ considerably between $BopE_{78-261}$ and the two *Salmonella* GEFs (Table 2).

The interactions between the two three-helix bundles of $BopE_{78-261}$ constitute an intricate network of charge and hydrophobic interactions. Among the residues involved are five arginine residues at sequence positions 100, 182, 200, 207 and 230 that are almost unique to BopE: SopE and SopE2 do not possess arginine residues in any of the corresponding positions (Supplementary Figure S1), but the putative bacterial GEF family member CopE from *Chromobacterium violaceum* (accession AAQ57975) has arginine residues corresponding to BopE Arg^{200} and Arg^{207}.Three of the BopE arginine residues, Arg^{200}, Arg^{207} and Arg^{230}, form part of the association between $\alpha5$- and $\alpha6$-helices, while Arg^{182} and Glu^{125} are suitably located to link $\alpha4$- and $\alpha2$-helices at the putative Cdc42-binding face (based on the $SopE_{78-240}$–Cdc42 complex structure [26]) of BopE through a potential salt bridge. Arg^{100} (in $\alpha1$-helix) occupies a hydrophobic pocket between $\alpha2$- and $\alpha5$-helices.

BopE residue Pro^{204} (corresponding to Ala^{199} in SopE and SopE2) promotes these interbundle interactions by disrupting $\alpha5$-helix into two parts termed $\alpha5'$ and $\alpha5''$. As a consequence, $\alpha5'$ is positioned to bridge the $\alpha1\alpha4\alpha5$ and $\alpha2\alpha3\alpha6$ bundles and its residues are able to interact with residues in $\alpha2$ and $\alpha6$ of the $\alpha2\alpha3\alpha6$ bundle (Figure 3).

In contrast with BopE Pro^{204}, three SopE/E2 proline residues appear to impede interbundle interaction and therefore contribute to the more open conformation adopted by $SopE2_{69-240}$ in solution relative to $BopE_{78-261}$. Near the apex of the Λ formed by the two three-helix bundles, the loop connecting $\alpha5$ and $\alpha6$ in $SopE2_{69-240}$ and $SopE_{78-240}$ bulges (Figure 3), presumably due to the presence of Pro^{211}, Pro^{219} and Pro^{221}. Due to the lack of proline residues at positions corresponding to 219 (Asn^{224} in BopE) and 221 (Leu^{226} in BopE), $BopE_{78-261}$ $\alpha6$-helix begins earlier in the amino acid sequence than SopE/E2 $\alpha6$ and the $BopE_{78-261}$ $\alpha5$–$\alpha6$ connecting element is a three-residue turn rather than the seven-residue loop observed in $SopE2_{69-240}$ and $SopE_{78-240}$ (Figure 3 and Supplementary Figure S1). We reason that this protrusion of the polypeptide chain in the $\alpha5$–$\alpha6$ loop at the apex of the Λ , not observed in $BopE_{78-261}$ due to the key amino acid differences described here, counteracts extensive interbundle interaction in $SopE_{78-240}$ and $SopE2_{69-240}$.

NMR investigation of the interaction between $BopE_{78-261}$ and Cdc42

In order to probe $BopE_{78-261}$ binding to Cdc42 in solution, 12 two-dimensional ^{1}H-^{15}N HQSC experiments on mixtures of varying ratios of uniformly ^{15}N-labelled $BopE_{78-261}$ and unlabelled human Cdc42Δ7 were performed. Two main types of behaviour were observed for peaks in $BopE_{78-261}$ HSQC spectra upon increasing the ratio of Cdc42Δ7 to $BopE_{78-261}$: general broadening of peaks characterized by intensity loss throughout the spectrum; and for more than one-third of residues, the appearance of one or more additional peaks per

backbone amide NH, indicating that BopE samples have more than one conformation upon interaction with Cdc42 with slow exchange between the conformations.

$BopE_{78-261}$ cross-peak broadening with increasing Cdc42Δ7 concentration— Almost all of the backbone NH peaks in ^{1}H-^{15}N HQSC spectra of $BopE_{78-261}$ broadened as a function of increasing Cdc42Δ7 concentration (Figure 4) until, at the highest Cdc42Δ7/$BopE_{78-261}$ ratio of 2.7:1, there was a subset of 15 peaks that remained relatively intense (14 of which can be assigned as Thr^{78}, Gly^{79}, Asp^{80}, Glu^{109}, Phe^{110}, Gly^{160}, Glu^{251}, Lys^{252}, Ala^{254}, Thr^{255}, Asn^{256}, Ala^{257}, Gly^{260} and Ala^{261} and hence comprise amino acids in presumably relatively flexible parts of the protein near the N- and C-termini plus the $\alpha1$–$\alpha2$ and pre-β-hairpin loops) plus a subset of readily detectable peaks [some of which can be assigned as Ala^{81}, Lys^{82}, Gln^{83}, Ala^{84} (all near the N-terminus), Asp^{162}, Gly^{165}, Val^{166} (β-hairpin), Gly^{190} ($\alpha4$–$\alpha5$ loop), Glu^{221} ($\alpha6$) and Ser^{248} (unstructured C-terminal region)] and about 40 further peaks that were still detectable just above the noise level. The remaining backbone NH peaks (in excess of 100) were broadened into the noise. Most asparagine and glutamine side-chain NH_2 cross-peaks were still present at the highest Cdc42Δ7/$BopE_{78-261}$ ratio of 2.7:1.0.

The rate of backbone NH peak broadening was reasonably uniform across the sequence, suggesting that the major contributors to broadening are the following: molecular mass increase upon complexation (a 1:1 $BopE_{78-261}$–Cdc42Δ7 complex is just over double the molecular mass of $BopE_{78-261}$), shape change upon complexation with potential for nonlinear increase in effective rotational correlation time, and exchange between free and bound $BopE_{78-261}$. Due to peak overlap, the degree and rate of broadening could not be quantified for a quarter of the approx. 175 backbone NH peaks. At a Cdc42Δ7/$BopE_{78-261}$ ratio of 1.0:1.0, many peaks were broadened to below 20 % of their original height with the greatest concentrations of less rapidly broadened peaks found at the terminal regions, particularly the C-terminal region (Figure 4). The highest concentration of particularly rapidly broadened peaks (to noise level at a Cdc42Δ7/$BopE_{78-261}$ ratio of 1.0:1.0) occurred in $\alpha2$-helix; the equivalent SopE helix is involved in the interface between $SopE_{78-240}$ and Cdc42 in the $SopE_{78-240}$-Cdc42 crystal structure [26].

Appearance of multiple cross-peaks per $BopE_{78-261}$ backbone NH—The second major observation upon increasing the Cdc42Δ7/ $BopE_{78-261}$ ratio was the appearance of a peak or peaks in addition to the original backbone NH peak for approx. 70 of the 175 backbone NH peaks; single extra peaks accounted for approx. 75 % of these 70 cases. In 56 instances, these additional peaks could be assigned to a particular amino acid by proximity to the corresponding original backbone NH peak. At least two of the 16 asparagine and glutamine side-chain NH_2 groups also displayed a second pair of peaks in the presence of Cdc42Δ7. In the vast majority of cases with one or more extra peaks, upon increasing the Cdc42Δ7/$BopE_{78-261}$ ratio the Cdc42Δ7-induced extra peaks increased in height or sometimes reached a plateau as the original backbone NH peaks decreased in height. The chemical shift difference between the original backbone NH peak and Cdc42Δ7-induced additional peak(s) at a Cdc42Δ7/$BopE_{78-261}$ ratio of 1.0:1.0 was calculated according to the formula $\Delta\delta_{ave} = [(\Delta\delta_{HN}^2+(\Delta\delta_N^2/25))/2]^{1/2}$, where $\Delta\delta_{HN}$ and $\Delta\delta_N$ correspond to the chemical shift difference in the amide ^{1}H and ^{15}N chemical shifts between the original NH peak and the Cdc42Δ7-induced extra peak(s); the $\Delta\delta_{ave}$ values are shown in Figure 5(A). In the cases where more than one Cdc42Δ7-induced extra peak could be assigned to a specific amino acid, the value plotted is the average of the $\Delta\delta_{ave}$ values. For 67 residues, only one backbone NH peak was observed throughout the titration; the approximate sequence positions of these residues are highlighted in Figure 5(A). For the remaining 40 or so backbone NH peaks, overlap hindered the observation of peak behaviour during the titration.

The presence of the Cdc42Δ7-induced additional peaks for residues in several parts of $BopE_{78-261}$ indicates that $BopE_{78-261}$ samples have more than one conformation in the presence of Cdc42Δ7 with the Cdc42Δ7-induced conformations in slow exchange with the initial Cdc42Δ7-free conformation. The fact that in approx. 75 % of cases with more than one NH peak the additional peak was a single peak indicates that one Cdc42Δ7-induced conformation was predominant. Clusters of residues exhibiting multiple backbone NH peaks are located in the $\alpha 1$–$\alpha 2$ loop and adjacent parts of $\alpha 1$ and $\alpha 2$, the β-hairpin and loops adjacent to the β-hairpin including the putative ^{171}GAGT^{174} catalytic motif, and around the $\alpha 5$–$\alpha 6$ loop (Figure 5). There is also a sequence of such residues in $\alpha 6$.

Comparison of $BopE_{78-261}$-Cdc42 and $SopE2_{69-240}$-Cdc42 titration results—

Very similar NMR titrations, both using Cdc42Δ7 and the same protocol, have now been carried out to study the $BopE_{78-261}$–Cdc42 (the present study) and $SopE2_{69-240}$–Cdc42 [27] interactions. $BopE_{78-261}$ and $SopE2_{69-240}$ both experienced widespread backbone NH peak broadening upon increasing the ratio of Cdc42Δ7 to $BopE_{78-261}$/$SopE2_{69-240}$. The broadening was, if anything, more rapid in the $SopE2_{69-240}$–Cdc42Δ7 titration. The $SopE2_{69-240}$ NH peaks that underwent Cdc42Δ7-induced chemical shift changes fall into two groups, one of which showed very good agreement with the $SopE_{78-240}$ residues involved in important intermolecular interactions in the $SopE_{78-240}$–Cdc42 crystal structure [26]: this group included $SopE2_{69-240}$ residues Gln^{109} ($\alpha 2$), Asp^{124} ($\alpha 2$), Gly^{165} (adjacent to catalytic motif), Gly^{166}, Gly^{168}, Ala^{169} (all catalytic motif), Val^{174} ($\alpha 4$), Gln^{194} ($\alpha 5$) and Lys^{198} ($\alpha 5$). The second group of perturbed $SopE2_{69-240}$ residues comprised several scattered internal residues and isolated residues on the opposite side of the molecule to the binding interface. In contrast with $SopE2_{69-240}$, slow exchange between unbound and Cdc42Δ7-bound conformations of $BopE_{78-261}$ was observed during the $BopE_{78-261}$–Cdc42Δ7 titration. The chemical shift differences between these states of $BopE_{78-261}$ were, in general, 4–5 or more times the magnitude of the Cdc42Δ7-induced chemical shift changes observed in the $SopE2_{69-240}$–Cdc42Δ7 titration. The BopE equivalents (BopE residues Asp^{128}, Gly^{171}, Gly^{173}, Thr^{174} and Thr^{179}) of five of the Cdc42-perturbed $SopE2_{69-240}$ residues ($SopE2_{69-240}$ residues Asp^{124}, Gly^{166}, Gly^{168}, Ala^{169} and Val^{174}) listed above were involved in the Cdc42-induced slow conformational exchange, whereas Ser^{170}, Tyr^{199} and Gln^{203}, the BopE equivalents of SopE residues Gly^{165}, Gln^{194} and Lys^{198}, were not. The behaviour of Gln^{113} (BopE equivalent of SopE Gln^{109}) during the titration could not be monitored due to peak overlap. Of the BopE equivalents of a further two $SopE_{78-240}$ residues that interact with Cdc42 in the $SopE_{78-240}$–Cdc42 crystal structure but that were not significantly perturbed in the $SopE2_{69-240}$–Cdc42Δ7 NMR titration [27], Ala^{135} ($\alpha 2$–$\alpha 3$ loop) was involved in the Cdc42-induced slow conformational exchange, but the behaviour of Asp^{107} could not be monitored due to peak overlap. The significance of the positions of slowly exchanging residues in $BopE_{78-261}$ is discussed in the next section.

Implications of $BopE_{78-261}$ tertiary structure and $BopE_{78-261}$–Cdc42 NMR titration for BopE interaction with Rho GTPases

The question arises as to whether the conformational difference between the catalytic domain of BopE and those of SopE and SopE2 has implications for interaction with Rho GTPases. Analysis of the interface between $SopE_{78-240}$ and Cdc42 in the $SopE_{78-240}$–Cdc42 complex crystal structure [26] reveals that the interaction can be broken down into two major components: a groove on $SopE_{78-240}$ accommodates a ridge on Cdc42 formed by residues 35–41 (switch region I) and the gap between the two three-helix bundles of $SopE_{78-240}$ accommodates Cdc42 residues Val^{36} and Asp^{38} (Supplementary Figure S2 at http://www.BiochemJ.org/bj/411/bj4110485add.htm). The latter interaction, in particular, indicates that, in its closed conformation, $BopE_{78-261}$ would experience steric clashes with Cdc42. The resulting implication is that BopE catalytic domain must undergo a change from

its closed conformation to a more open conformation like those of SopE and SopE2 catalytic domains in order to carry out its guanine nucleotide-exchange function. A requirement for such a large-scale conformational change is consistent with, and may at least partially explain, the observed differences in catalytic-centre activity for guanine nucleotide exchange between $BopE_{78-261}$ and its *Salmonella* counterparts: a k_{cat} of 0.48 s^{-1} was measured for $BopE_{78-261}$-induced guanine nucleotide exchange in Rac1 (a similar rate was measured for Cdc42) [20], whereas the k_{cat} values for guanine nucleotide exchange in Cdc42 are 5±1 and 19±3s^{-1} for $SopE_{78-240}$ and $SopE2_{69-240}$ respectively [25].

It might then be asked whether BopE catalytic domain exists in equilibrium in solution between closed and open forms or whether it undergoes a conformational change upon interaction with the target protein. These two possibilities are not necessarily mutually exclusive – there may be equilibrium in solution for unbound BopE catalytic domain but one that lies strongly towards the closed conformation. The results of the $BopE_{78-261}$–Cdc42Δ7 titration are consistent with a significant conformational change in $BopE_{78-261}$ upon binding to Cdc42: when superimposed on the structure of $BopE_{78-261}$ (Figure 5B), it is apparent that many of the amino acids that sampled one or more Cdc42Δ7-induced conformations during the $BopE_{78-261}$–Cdc42Δ7 titration are located in potential hinge areas for a closed-to-open conformational change involving relative reorientation of the two three-helix bundles of $BopE_{78-261}$. These hinge areas include the α1–α2 loop and adjacent residues in α1 and α2, residues in the region between α3 and α4 that includes the β-hairpin and $G^{171}AGT^{174}$ putative catalytic motif, and residues in and around the α5–α6 turn. Residues in the central part of α2 also show slow exchange between initial and Cdc42Δ7-induced conformations, consistent with a change in conformation and/or position of the α3–α4 loop C-terminal to the β-hairpin that associates with this part of α2 in Cdc42-free $BopE_{78-261}$ (Figure 1). It is also striking that a few of the amino acids with multiple NH peaks are located in areas that would be involved in any intrabundle conformational changes, suggesting that the three-helix bundles themselves remain largely unchanged. The considerably greater magnitude of the Cdc42Δ7-induced chemical shift differences between free and Cdc42Δ7-bound states of $BopE_{78-261}$ compared with the magnitude of the chemical shift changes observed in the $SopE2_{69-240}$–Cdc42Δ7 titration underpins the conclusion that $BopE_{78-261}$ undergoes greater structural change than $SopE2_{69-240}$ upon binding of the Rho GTPase.

Guanine nucleotide-exchange activity of $BopE_{78-261}$ and $BopE_{78-261}$ mutants

In order to investigate further the requirement for a conformational change in BopE for catalysis of nucleotide exchange in Rho GTPases, three $BopE_{78-261}$ double mutants were made. These were N224P/R230Q (mutant 1), N216P/L226P (mutant 2) and R207E/N216P (mutant 3). The mutations were selected according to their potential for changing $BopE_{78-261}$ from its relatively closed conformation to a more open conformation closer to those observed for $SopE_{78-240}$ in its complex with Cdc42 [26] and unbound $SopE2_{69-240}$ [27], as follows: N224P to induce a SopE/E2-like bulge in the α5–α6 loop; R230Q to further disrupt the α5–α6 interaction; N216P and L226P to induce a SopE/E2-like bulge in the α5–α6 loop; R207E to disrupt the α5–α6 interaction and N216P to induce a SopE/E2-like bulge in the α5–α6 loop.

Like the wild-type recombinant $BopE_{78-261}$, the mutants were cloned and expressed as GST (glutathione transferase) fusions. Mutant 1 was expressed relatively poorly in *E. coli*, but could be purified; mutant 2 was expressed at low levels, but disappeared during purification (perhaps this mutant is misfolded and therefore rapidly degraded); and mutant 3 was expressed well and could be purified. In filter binding assays [49] with BSA as the negative control, the order of nucleotide exchange catalytic efficiency was: $BopE_{78-261}$ N224P/R230Q (mutant 1)>$SopE2_{69-240}$>wild-type $BopE_{78-261}$≫$BopE_{78-261}$ R207E/N216P (mutant 3); in fact, mutant 3 showed essentially no catalytic activity (Figure 6). The reason for the

lack of nucleotide-exchange activity in mutant 3 is unclear, but the R207E/N216P double mutation obviously induces changes that disrupt rather than enhance BopE function. The N224P/R230Q double mutation in $BopE_{78-261}$, on the other hand, produces a much more effective GEF than wild-type $BopE_{78-261}$ and a better GEF than even $SopE2_{69-240}$ (Figure 6), itself a better GEF for Cdc42 than $SopE_{78-240}$ [25]. This result, showing that mutations designed to abrogate important interbundle interactions and thereby induce a more open conformation in $BopE_{78-261}$ can substantially improve nucleotide-exchange catalytic efficiency, adds further strong experimental support to that from NMR titration for the hypothesis that BopE GEF domain undergoes Rho GTPase-induced change from a closed to an open conformation.

Conclusions

The molecular mechanisms of *B. pseudomallei* pathogenesis are not well understood. A number of putative type III secreted effector proteins have been identified by analysis of the *B. pseudomallei* genome sequence [15]. One of these proteins, BopE, is a homologue of the potent GEFs SopE [21,50] and SopE2 [23,24] from *Salmonella enterica* (Supplementary Figure S1). SopE and SopE2 catalyse nucleotide exchange in mammalian Rho GTPases, contributing to disruption of the host cell membrane and invasion of the host cell [17,21,23,25,50,51]. BopE, likewise, acts as a GEF for the Rho GTPases Cdc42 and Rac1 *in vitro* and may play a role in the invasion of non-phagocytic epithelial cells [20]. The present study shows that BopE and SopE/SopE2 catalytic domains adopt similar three-dimensional folds comprising two three-helix bundles but also shows that BopE has a more compact conformation, involving significant interbundle interactions, than its *Salmonella* homologues. The most open conformation of the three is for Cdc42-bound $SopE_{78-240}$, with unbound $SopE2_{69-240}$ slightly more closed. It is worth noting, however, that SopE residues involved in contacting Cdc42 in the $SopE_{78-240}$–Cdc42 complex crystal structure [26] are largely conserved or conservatively substituted in BopE (Supplementary Figure S1). SopE residues (Asp^{103}, Gln^{109}, Asp^{124} and Gly^{168}) shown by mutation to be functionally important [31] are, moreover, conserved in BopE. It seems likely, therefore, that despite its more closed conformation, BopE ultimately utilizes the same mechanism as SopE and other Rho GEFs [52] in catalysing guanine nucleotide exchange in Rho GTPases. This would require that BopE change from closed to open conformations in the presence of Rho GTPase target proteins. Such a conformational change is evidenced here by the results of a $BopE_{78-261}$–Cdc42 NMR titration and measurements of nucleotide-exchange catalytic efficiency comparing wild-type and mutant BopE GEF domain. Phosphorylation of BopE would not seem to be required for any conformational change as we and others have shown that $BopE_{78-261}$ purified from *E. coli* exhibits GEF activity [20]. Finally, given the sequence and conformational differences between BopE and SopE/E2 catalytic domains, it is possible that there are as yet unknown differences in specificity among the members of this family of bacterial GEFs, with the potential for modulation of the activities of small G-proteins in addition to Cdc42 and Rac1.

Supplementary Material

Refer to Web version on PubMed Central for supplementary material.

Acknowledgments

This work was supported at the University of Bath by The Wellcome Trust (grant no. 060998) and at IAH by the BBSRC (Biotechnology and Biological Sciences Research Council). The Wellcome Trust is acknowledged for purchase of the 600 MHz NMR spectrometer (grant no. 051902) used in this study. C.W. was supported by a Ph.D. studentship from the EPSRC (Engineering and Physical Sciences Research Council; U.K.). We thank Dr Julian Eaton (Department of Biology and Biochemistry, University of Bath, Bath, U.K.) for constructive criticism of this paper and help with RMSD calculations, Professor Lewis Kay (Department of Biochemistry, University of Toronto,

Toronto, ON, Canada) for some of the pulse sequences used here, Dr Charles Schwieters (Center for Information Technology, National Institutes of Health Bethesda, MD, U.S.A.) for help with the Python interface of Xplor-NIH, Dr Kyoko Yap (Department of Structural and Chemical Biology, Mount Sinai School of Medicine, New York, NY, U.S.A.) for the program Interhlx, Graham Pavitt's group (Faculty of Life Sciences, University of Manchester, Manchester, U.K.) for instructions on filter binding assays and Mareike Posner (Department of Biology and Biochemistry, University of Bath, Bath, U.K.) for advice on enzyme assays.

Abbreviations used:

Cdc42	cell division cycle 42
for	forward
GEF	guanine-nucleotide-exchange factor
HSQC	heteronuclear single-quantum coherence
NOE	nuclear Overhauser effect
rev	reverse
RDC	residual dipolar coupling
RMSD	root mean square deviation
TTS system	type III secretion system

REFERENCES

1. Dance DAB. Melioidosis. Curr. Opin. Infect. Dis. 2002; 15:127–132. [PubMed: 11964912]
2. White NJ. Melioidosis. Lancet. 2003; 361:1715–1722. [PubMed: 12767750]
3. Peacock SJ. Melioidosis. Curr. Opin. Infect. Dis. 2006; 19:421–428. [PubMed: 16940864]
4. Brett PJ, Woods DE. Pathogenesis of and immunity to melioidosis. Acta Tropica. 2000; 74:201–210. [PubMed: 10674650]
5. Currie BJ, Fisher DA, Howard DM, Burrow JNC, Lo D, Selva-Nayagam S, Anstey NM, Huffam SE, Snelling PL, Marks PJ, et al. Endemic melioidosis in tropical northern Australia: a 10-year prospective study and review of the literature. Clin. Infect. Dis. 2000; 31:981–986. [PubMed: 11049780]
6. Currie BJ, Fisher DA, Anstey NM, Jacups SP. Melioidosis: acute and chronic disease, relapse and re-activation. Trans. R. Soc. Trop. Med. Hyg. 2000; 94:301–304. [PubMed: 10975006]
7. Chaowagul W, Suputtamongkol Y, Dance DAB, Rajchanuvong A, Pattaraarechachai J, White NJ. Relapse in melioidosis – incidence and risk factors. J. Infect. Dis. 1993; 168:1181–1185. [PubMed: 8228352]
8. Wilkinson L. Glanders: medicine and veterinary medicine in common pursuit of a contagious disease. Med. Hist. 1981; 25:363–384. [PubMed: 7038356]
9. Rotz L, Khan A, Lillibridge S, Ostroff S, Hughes J. Public health assessment of potential biological terrorism agents. Emerg. Infect. Dis. 2002; 8:225–230. [PubMed: 11897082]
10. Haque A, Chu K, Easton A, Stevens MP, Galyov EE, Atkins T, Titball R, Bancroft GJ. A live experimental vaccine against *Burkholderia pseudomallei* elicits CD4(+) T cell-mediated immunity, priming T cells specific for 2 type III secretion system proteins. J. Infect. Dis. 2006; 194:1241–1248. [PubMed: 17041850]
11. Stevens MP, Galyov EE. Exploitation of host cells by *Burkholderia pseudomallei*. Int. J. Med. Microbiol. 2004; 293:549–555. [PubMed: 15149030]
12. Holden MTG, Titball RW, Peacock SJ, Cerdeno-Tarraga AM, Atkins T, Crossman LC, Pitt T, Churcher C, Mungall K, Bentley SD, et al. Genomic plasticity of the causative agent of melioidosis, *Burkholderia pseudomallei*. Proc. Natl. Acad. Sci. U.S.A. 2004; 101:14240–14245. [PubMed: 15377794]

13. Rainbow L, Hart CA, Winstanley G. Distribution of type III secretion gene clusters in *Burkholderia pseudomallei, B. thailandensis* and *B. mallei*. J. Med. Microbiol. 2002; 51:374–384. [PubMed: 11990489]
14. Attree O, Attree I. A second type III secretion system in *Burkholderia pseudomallei*: who is the real culprit? Microbiology. 2001; 147:3197–3199. [PubMed: 11739751]
15. Stevens MP, Wood MW, Taylor LA, Monaghan P, Hawes P, Jones PW, Wallis TS, Galyov EE. An inv/mxi-spa-like type III protein secretion system in *Burkholderia pseudomallei* modulates intracellular behaviour of the pathogen. Mol. Microbiol. 2002; 46:649–659. [PubMed: 12410823]
16. Johnson S, Deane JE, Lea SM. The type III needle and the damage done. Curr. Opin. Struct. Biol. 2005; 15:700–707. [PubMed: 16263265]
17. Galàn JE, Wolf-Watz H. Protein delivery into eukaryotic cells by type III secretion machines. Nature. 2006; 444:567–573. [PubMed: 17136086]
18. Cornelis GR, Van Gijsegem F. Assembly and function of type III secretory systems. Annu. Rev. Microbiol. 2000; 54:735–774. [PubMed: 11018143]
19. Pallen MJ, Beatson SA, Bailey CM. Bioinformatics, genomics and evolution of non-flagellar type-III secretion systems: a Darwinian perspective. FEMS Microbiol. Rev. 2005; 29:201–229. [PubMed: 15808742]
20. Stevens MP, Friebel A, Taylor LA, Wood MW, Brown PJ, Hardt W-D, Galyov EE. A *Burkholderia pseudomallei* type III secreted protein, BopE, facilitates bacterial invasion of epithelial cells and exhibits guanine nucleotide exchange factor activity. J. Bacteriol. 2003; 185:4992–4996. [PubMed: 12897019]
21. Wood MW, Rosqvist R, Mullan PB, Edwards MH, Galyov EE. SopE, a secreted protein of *Salmonella dublin*, is translocated into the target eukaryotic cell via a Sip-dependent mechanism and promotes bacterial entry. Mol. Microbiol. 1996; 22:327–338. [PubMed: 8930917]
22. Hardt WD, Chen LM, Schuebel KE, Bustelo XR, Galàn JE. *S. typhimurium* encodes an activator of Rho GTPases that induces membrane ruffling and nuclear responses in host cells. Cell. 1998; 93:815–826. [PubMed: 9630225]
23. Bakshi CS, Singh VP, Wood MW, Jones PW, Wallis TS, Galyov EE. Identification of SopE2, a *Salmonella* secreted protein which is highly homologous to SopE and involved in bacterial invasion of epithelial cells. J. Bacteriol. 2000; 182:2341–2344. [PubMed: 10735884]
24. Stender S, Friebel A, Linder S, Rohde M, Mirold S, Hardt WD. Identification of SopE2 from *Salmonella typhimurium*, a conserved guanine nucleotide exchange factor for Cdc42 of the host cell. Mol. Microbiol. 2000; 36:1206–1221. [PubMed: 10931274]
25. Friebel A, Ilchmann H, Aelpfelbacher M, Ehrbar K, Machleidt W, Hardt WD. SopE and SopE2 from *Salmonella typhimurium* activate different sets of Rho GTPases of the host cell. J. Biol. Chem. 2001; 276:34035–34040. [PubMed: 11440999]
26. Buchwald G, Friebel A, Galàn JE, Hardt WD, Wittinghofer A, Scheffzek K. Structural basis for the reversible activation of a Rho protein by the bacterial toxin SopE. EMBO J. 2002; 21:3286–3295. [PubMed: 12093730]
27. Williams C, Galyov EE, Bagby S. Solution structure, backbone dynamics, and interaction with Cdc42 of *Salmonella* guanine nucleotide exchange factor SopE2. Biochemistry. 2004; 43:11998–12008. [PubMed: 15379540]
28. Cerione RA, Zheng Y. The Dbl family of oncogenes. Curr. Opin. Cell Biol. 1996; 8:216–222. [PubMed: 8791419]
29. Snyder JT, Worthylake DK, Rossman KL, Betts L, Pruitt WM, Siderovski DP, Der CJ, Sondek J. Structural basis for the selective activation of Rho GTPases by Dbl exchange factors. Nat. Struct. Biol. 2002; 9:468–475. [PubMed: 12006984]
30. Rehmann H, Wittinghofer A, Bos JL. Capturing cyclic nucleotides in action: snapshots from crystallographic studies. Nat. Rev. Mol. Cell Biol. 2007; 8:63–73. [PubMed: 17183361]
31. Schlumberger MC, Friebel A, Buchwald G, Scheffzek K, Wittinghofer A, Hardt W-D. Amino acids of the bacterial toxin SopE involved in G nucleotide exchange on Cdc42. J. Biol. Chem. 2003; 278:27149–27159. [PubMed: 12719429]
32. Upadhyay A, Williams C, Gill AC, Philippe DL, Davis K, Taylor LA, Stevens MP, Galyov EE, Bagby S. Biophysical characterization of the catalytic domain of guanine nucleotide exchange

factor BopE from *Burkholderia pseudomallei*. Biochim. Biophys. Acta. 2004; 1698:111–119. [PubMed: 15063321]

33. Wu H-L, Williams C, Upadhyay A, Galyov EE, Bagby S. Assignment of the ^{1}H, ^{13}C and ^{15}N resonances of the catalytic domain of guanine nucleotide exchange factor BopE from *Burkholderia pseudomallei*. J. Biomol. NMR. 2004; 29:215–216. [PubMed: 15014239]
34. Delaglio F, Grzesiek S, Vuister GW, Zhu G, Pfeifer J, Bax A. NMRPipe: a multidimensional spectral processing system based on Unix pipes. J. Biomol. NMR. 1995; 6:277–293. [PubMed: 8520220]
35. Reference deleted
36. Macura S, Ernst RR. Elucidation of cross-relaxation in liquids by two-dimensional NMR spectroscopy. J. Phys. 1980; 41:95–117.
37. Zhang OW, Kay LE, Olivier JP, Forman-Kay JD. Backbone ^{1}H and ^{15}N resonance assignments of the N-terminal SH3 domain of drk in folded and unfolded states using enhanced-sensitivity pulsed-field gradient NMR techniques. J. Biomol. NMR. 1994; 4:845–858. [PubMed: 7812156]
38. Pascal SM, Muhandiram DR, Yamazaki T, Forman-Kay JD, Kay LE. Simultaneous acquisition of ^{15}N-edited and ^{13}C-edited NOE spectra of proteins dissolved in H_2O. J. Magn. Reson. Ser. B. 1994; 103:197–201.
39. Chou JJ, Gaemers S, Howder B, Louis JM, Bax A. A simple apparatus for generating stretched polyacrylamide gels, yielding uniform alignment of proteins and detergent micelles. J. Biomol. NMR. 2001; 21:377–382. [PubMed: 11824758]
40. Ottiger M, Delaglio F, Bax A. Measurement of J and dipolar couplings from simplified two-dimensional NMR spectra. J. Magn. Reson. 1998; 131:373–378. [PubMed: 9571116]
41. Nilges M. A calculation strategy for the structure determination of symmetrical dimers by ^{1}H NMR. Proteins: Struct. Funct. Genet. 1993; 17:297–309. [PubMed: 8272427]
42. Cornilescu G, Delaglio F, Bax A. Protein backbone angle restraints from searching a database for chemical shift and sequence homology. J. Biomol. NMR. 1999; 13:289–302. [PubMed: 10212987]
43. Schwieters CD, Kuszewski JJ, Tjandra N, Clore GM. The Xplor-NIH NMR molecular structure determination package. J. Magn. Reson. 2003; 160:65–73. [PubMed: 12565051]
44. Schwieters CD, Kuszewski JJ, Clore GM. Using Xplor-NIH for NMR molecular structure determination. Prog. Nucl. Magn. Res. Spectrosc. 2006; 48:47–62.
45. Schwieters CD, Clore GM. The VMD-Xplor visualization package for NMR structure refinement. J. Magn. Reson. 2001; 149:239–244. [PubMed: 11318623]
46. Laskowski RA, Rullmann JAC, MacArthur MW, Kaptein R, Thornton JM. AQUA and PROCHECK-NMR: programs for checking the quality of protein structures solved by NMR. J. Biomol. NMR. 1996; 8:477–486. [PubMed: 9008363]
47. Rudolph MG, Weise C, Mirold S, Hillenbrand B, Bader B, Wittinghofer A, Hardt WD. Biochemical analysis of SopE from *Salmonella typhimurium*, a highly efficient guanosine nucleotide exchange factor for Rho GTPases. J. Biol. Chem. 1999; 274:30501–30509. [PubMed: 10521431]
48. McAlister MSB, Mott HR, van der Merwe PA, Campbell ID, Davis SJ, Driscoll PC. NMR analysis of interacting soluble forms of the cell–cell recognition molecules CD2 and CD48. Biochemistry. 1996; 35:5982–5991. [PubMed: 8634239]
49. Self AJ, Hall A. Measurement of intrinsic nucleotide exchange and GTP hydrolysis rates. Methods Enzymol. 1995; 256:67–76. [PubMed: 7476456]
50. Hardt WD, Chen LM, Schuebel KE, Bustelo XR, Galàn JE. *Typhimurium* encodes an activator of Rho GTPases that induces membrane ruffling and nuclear responses in host cells. Cell. 1998; 93:815–826. [PubMed: 9630225]
51. Friebel A, Hardt WD. Purification and biochemical activity of *Salmonella* exchange factor SopE. Meth. Enzymol. 2000; 325:82–91. [PubMed: 11036594]
52. Thomas C, Fricke I, Scrima A, Berken A, Wittinghofer A. Structural evidence for a common intermediate in small G protein–GEF reactions. Mol. Cell. 2007; 25:141–149. [PubMed: 17218277]

Europe PMC Funders Author Manuscripts

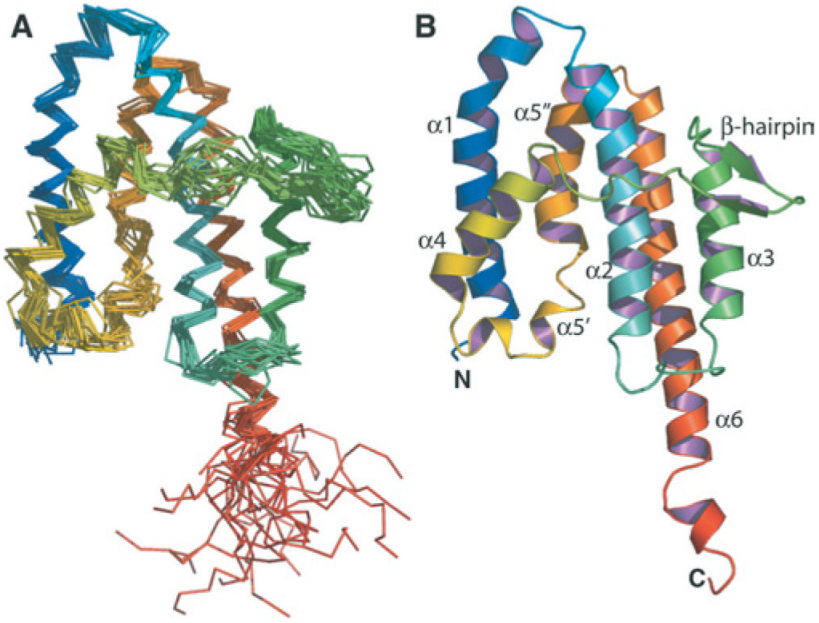

Figure 1. Structure of the BopE GEF domain (residues 78–261)

(**A**) Backbone (N, C^{α} and C') trace of the 20 lowest energy structures coloured as a continuum from blue at the N-terminus to red at the C-terminus. (**B**) Ribbon diagram of the average structure coloured as in (**A**). The α-helices and β-hairpin are labelled. The $G^{171}AGT^{174}$ putative catalytic motif lies between the β-hairpin and $\alpha 4$.

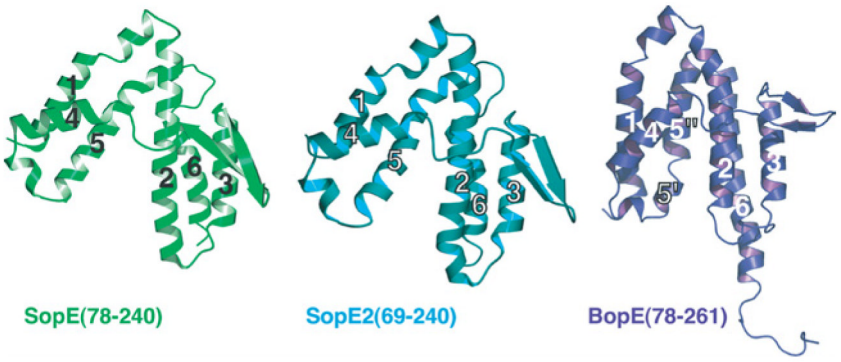

Figure 2. Comparison of the structures of SopE, SopE2 and BopE catalytic GEF domains

Representations of the crystal structure of Cdc42-bound $SopE_{78-240}$ (green; PDB code 1GZS), solution structure of $SopE2_{69-240}$ (cyan; PDB codes 1R6E and 1R9K) and solution structure of $BopE_{78-261}$ (purple; PDB codes 2JOK and 2JOL), demonstrating the similarities and differences in the $SopE_{78-240}$, $SopE2_{69-240}$ and $BopE_{78-261}$ structures. All three structures consist of two three-helix bundles with a connecting β-hairpin that is followed by a loop that contains the $G^{166}AGA^{169}$ (SopE/E2)/$G^{171}AGT^{174}$ (BopE) catalytic motif.

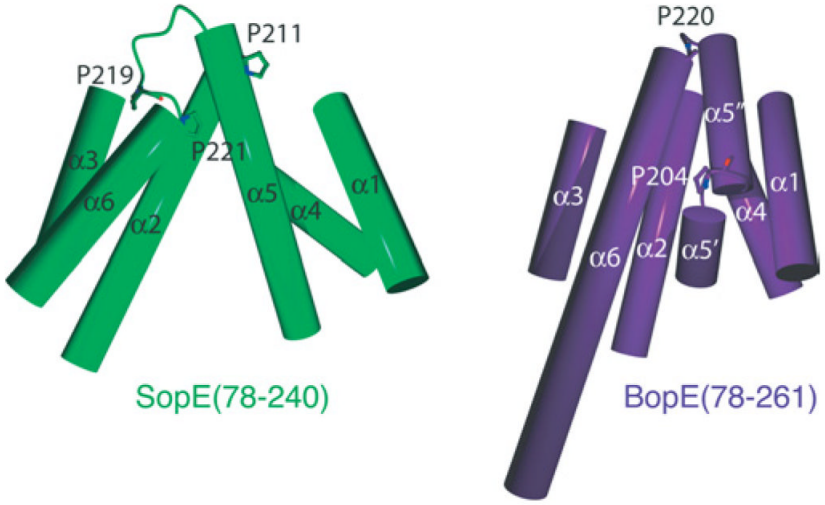

Figure 3. Comparison of SopE$_{78-240}$ and BopE$_{78-261}$ conformations

In order to highlight the major secondary structure and conformational differences between SopE$_{78-240}$ (green) and BopE$_{78-261}$ (purple), the α-helices of the two structures are shown and the locations of relevant proline residues are highlighted. Note the contrast between the protuberance of the $\alpha5$–$\alpha6$ loop in SopE$_{78-240}$ due to Pro^{211}, Pro^{219} and Pro^{221} and the compactness of the corresponding turn in BopE$_{78-261}$. Also note the disruption of BopE$_{78-261}$ $\alpha5$-helix by Pro^{204} into two parts, labelled $\alpha5'$ and $\alpha5''$, which permits $\alpha5'$ in particular to interact with the $\alpha2\alpha3\alpha6$ bundle. Both characteristics arise from the presence or absence of proline residues and result in the greater compactness of BopE$_{78-261}$ relative to SopE$_{78-240}$ and SopE2$_{69-240}$. The viewpoint for this Figure is approx. 180° different from that used for Figures 1 and 2.

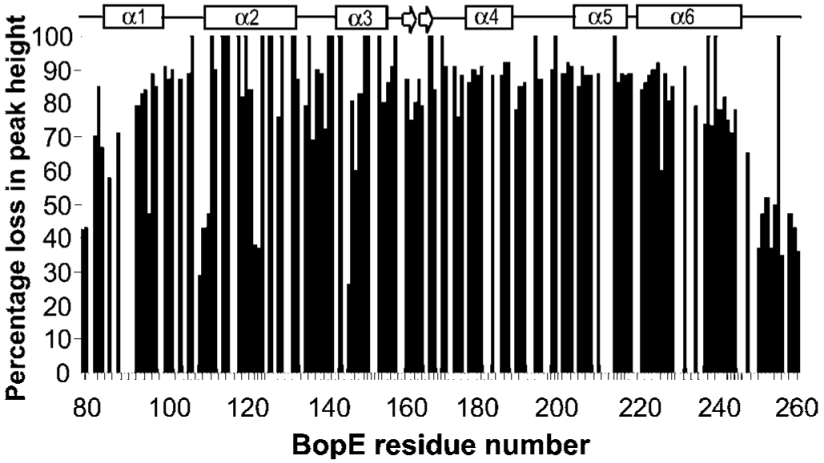

Figure 4. Reduction in BopE$_{78-261}$ backbone NH peak height as a function of BopE residue number upon titration with Cdc42Δ7

The percentage reduction in peak height is shown at a BopE$_{78-261}$/Cdc42Δ7 molar ratio of 1.0:1.0. Only one BopE$_{78-261}$ residue, Cys^{131}, showed no reduction in peak height. For the remainder of the residues that appear with 0% reduction on this plot, peak height could not be quantified due to peak overlap. Note that proline residues, which do not give rise to peaks in ^{1}H-^{15}N HSQC spectra and so are not monitored in this titration, occur at BopE$_{78-261}$ sequence positions 102, 134, 143, 159, 169, 176, 197, 204 and 219.

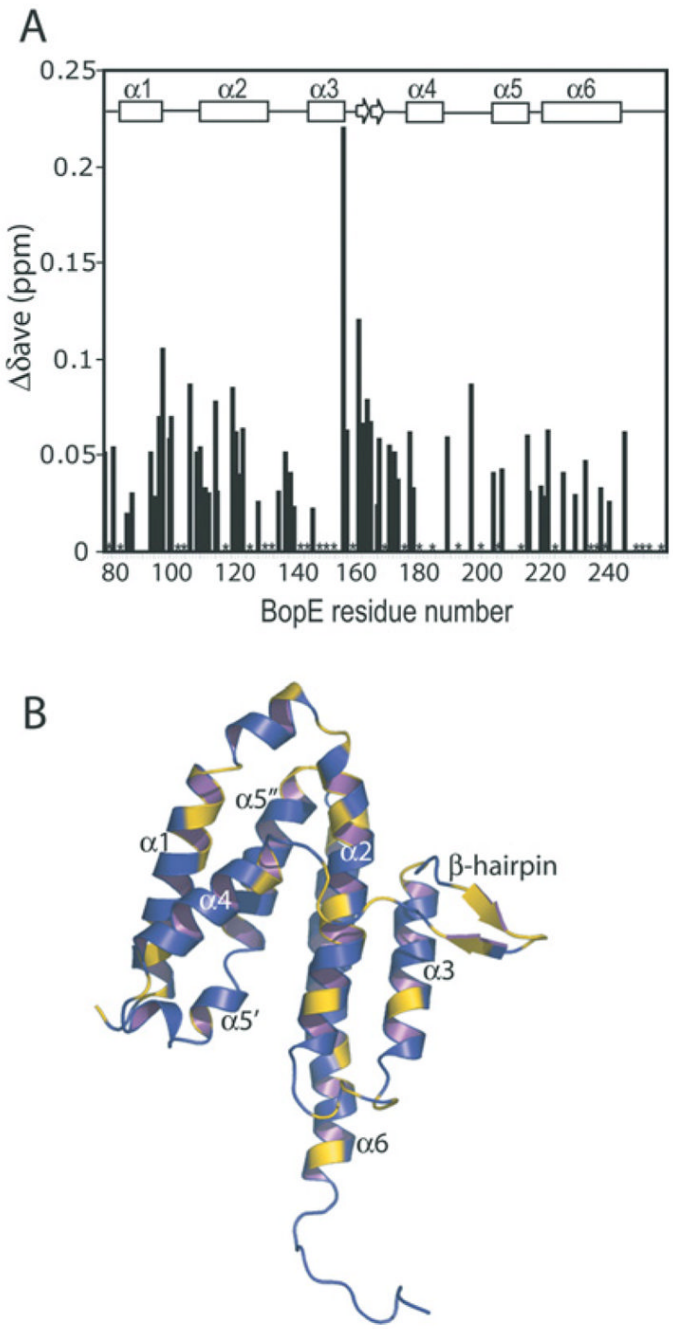

Figure 5. BopE$_{78-261}$ residues that show slow conformational exchange in the presence of Cdc42Δ7

(**A**) Average chemical shift differences plotted as a function of BopE residue number. The values were calculated using $\Delta\delta_{ave}=[(\Delta\delta_{HN}^2+(\Delta\delta_N^2/25))/2]^{1/2}$, where $\Delta\delta_{HN}$ and $\Delta\delta_N$ correspond to the chemical shift difference in the amide proton and ^{15}N chemical shifts between the original NH peak and the Cdc42Δ7-induced extra peak(s). The approximate sequence positions of the 67 residues for which only one backbone NH peak was observed are indicated by asterisks. (**B**) The average structure of BopE$_{78-261}$. Amino acids for which one or more additional backbone NH peaks appeared in BopE$_{78-261}$ ^{1}H-^{15}N HSQC spectra

during the $BopE_{78-261}$-Cdc42Δ7 titration are shown in yellow and the remainder are shown in purple.

Europe PMC Funders Author Manuscripts

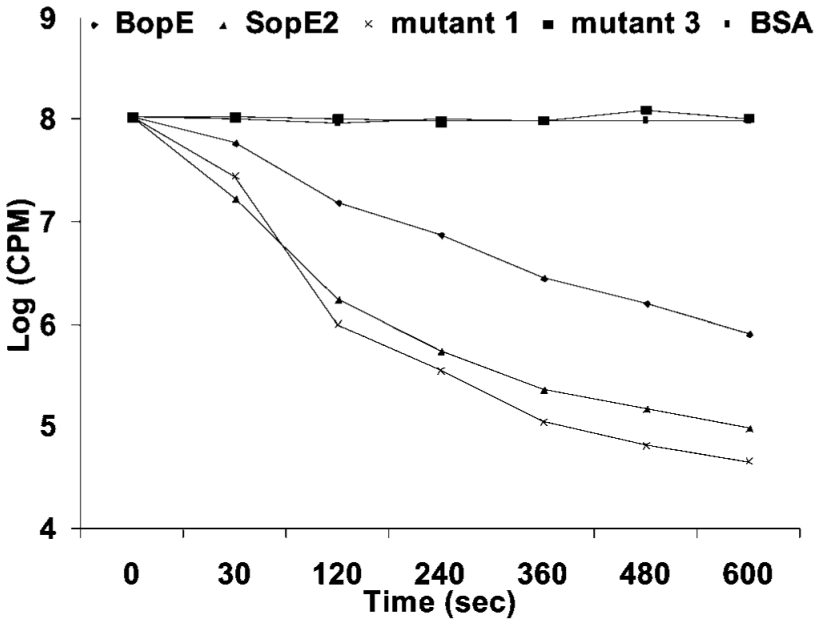

Figure 6. Kinetic analysis by filter binding assay of guanine nucleotide exchange in Cdc42 mediated by $BopE_{78-261}$, $BopE_{78-261}$ mutants and $SopE2_{69-240}$

Radioactivity was measured as c.p.m. The logarithm of the radioactivity [Log (CPM)] was plotted against time and the gradient of a best-fit line was taken as a measure of guanine nucleotide-exchange efficiency (rate of change in radioactivity as a function of time). The catalytic efficiency rank is: $BopE_{78-261}$ N224P/R230Q (mutant 1; gradient −0.5831)>$SopE2_{69-240}$ (gradient −0.5038)> wild-type $BopE_{78-261}$ (gradient −0.3658)>>$BopE_{78-261}$ R207E/N216P (mutant 3) and BSA (for both, gradient 0.0038). $BopE_{78-261}$ N224P/R230Q (mutant 1) is therefore a better catalyst of guanine nucleotide exchange in Cdc42 than $SopE2_{69-240}$ and a much better catalyst than wild-type $BopE_{78-261}$.

Table 1
Structural statistics on NMR-derived structures of BopE GEF domain

The RMSD from the mean structure calculated over residues 83–99, 110–133, 143–156, 177–189, 205–217 and 220–246. Ramachandran plot regions were calculated with PROCHECK-NMR [46].

(a)

Parameter	Value
Total number of NOE restraints	2452
Intraresidue	784
Sequential/median range (*i* to *i*+1−4)	1151
Long range	517
Number of dihedral angle restraints	255
Number of hydrogen bond restraints	192
Number of backbone $^{1}D_{NH}$ RDC restraints	98
RMSD for backbone atoms (Å)	0.65
RMSD for non-hydrogen atoms (Å)	1.15
Average numbers of NOE violations (per structure)	
>0.3 Å	5
>0.5 Å	1
Average number of dihedral angle violations (per structure)	
>5°	0

(b)

	Value (%)	
Ramachandran plot regions	Average structure	Ensemble
Most favoured	88.8	80.8
Additional allowed	8.7	15.9
Generously allowed	1.9	2.6
Disallowed	0.6	0.7

Europe PMC Funders Author Manuscripts

Table 2

Comparison of helix crossing angles in the solution structures of $BopE_{78-261}$ and $SopE_{69-240}$ and the crystal structure of Cdc42-bound $SopE_{78-240}$

Helix pair	Crossing angle (Å)*					
	$BopE_{78-261}$	$SopE2_{69-240}$†	$SopE_{78-240}$‡	Δ1§	Δ2//	Δ3¶
1–2	155.68	144.63	140.08	11.05	15.60	4.55
1–3	−35.28	−39.37	−44.45	4.09	9.17	5.08
1–4	137.08	131.03	132.95	6.05	4.13	−1.92
1–5	−21.02	−37.61	−34.47	16.59	13.45	3.14
1–6	152.68	133.14	126.04	19.54	26.64	7.10
2–3	167.18	159.41	165.24	7.77	1.94	5.83
2–4	−49.60	−77.02	−79.58	27.42	29.98	2.56
2–5	−158.43	−134.98	−133.83	−23.45	−24.60	−1.15
2–6	−3.46	−16.15	−14.14	12.69	10.68	−2.01
3–4	131.60	114.21	105.35	17.39	26.25	8.86
3–5	−24.31	28.47	37.81	−52.78	−62.12	−9.34
3–6	170.61	166.69	163.04	3.92	7.57	3.65
4–5	151.66	141.47	142.39	10.19	9.27	−0.92
4–6	−49.40	−78.97	−90.72	29.57	41.32	11.75
5–6	157.99	138.28	125.41	19.71	32.58	12.87

*Calculated with the program Interhlx (Kyoko Yap, University of Toronto; http://nmr.uhnres.utoronto.ca/ikura/interhlx).

†SopE2 GEF domain NMR structure (PDB entry 1R9K).

‡SopE GEF domain crystal structure (PDB entry 1GZS).

§The $BopE_{78-261}$ helix crossing angle minus the $SopE2_{69-240}$ helix crossing angle.

//The $BopE_{78-261}$ helix crossing angle minus the $SopE_{78-240}$ helix crossing angle.

¶The $SopE2_{69-240}$ helix crossing angle minus the $SopE_{78-240}$ helix crossing angle.